

Ultrastrong-coupling effects induced by a single classical drive in Jaynes-Cummings-type systems

Carlos Sánchez Muñoz,^{1,2} Anton Frisk Kockum,^{1,3} Adam Miranowicz,^{1,4} and Franco Nori^{1,5}

¹Theoretical Quantum Physics Laboratory, RIKEN Cluster for Pioneering Research, Wako-shi, Saitama 351-0198, Japan

²Clarendon Laboratory, University of Oxford, Parks Road, Oxford OX1 3PU, United Kingdom

³Wallenberg Centre for Quantum Technology, Department of Microtechnology and Nanoscience, Chalmers University of Technology, 412 96 Gothenburg, Sweden

⁴Faculty of Physics, Adam Mickiewicz University, 61-614 Poznań, Poland

⁵Department of Physics, The University of Michigan, Ann Arbor, Michigan 48109-1040, USA

(Dated: May 17, 2022)

We propose the effective simulation of light-matter ultrastrong-coupling phenomena with strong-coupling systems. Recent theory and experiments have shown that the single-atom quantum Rabi model can be simulated by the Jaynes-Cummings model with *two* additional classical drives. Here, we show that quantum nonlinear optical phenomena, relying on the counter-rotating terms of the Rabi model, can be implemented by the Jaynes-Cummings and Tavis-Cummings models with only a *single* classical drive. We analyze three examples: a single atom exciting two photons, frequency conversion, and a single photon exciting two atoms.

Introduction.—The ultrastrong coupling (USC) of light and matter is attracting increasing interest beyond the fields of cavity [1] and circuit [2, 3] quantum electrodynamics (QED) [4, 5]. This interest has been stimulated in the last decade by several experiments finally reaching USC in a variety of physical systems, e.g. superconducting quantum circuits, intersubband polaritons, Landau polaritons, organic molecules, and quantum optomechanical systems [4, 5]. The USC of light and matter (e.g., a cavity mode and a natural or artificial atom) occurs when their coupling strength g becomes comparable to the atomic (ω_a) or cavity (ω_c) frequencies. More precisely, according to the usual convention, the USC regime occurs when $\eta = \max(g/\omega_c, g/\omega_a)$ is in the range $[0.1, 1)$. The regime $\eta \geq 1$ is often referred to as deep strong coupling (DSC) [6].

Compared to strong coupling (SC; $\eta < 0.1$, but g larger than the loss rates in the system), USC opens new perspectives for efficiently simulating known effects and observing fundamentally new phenomena in quantum nonlinear optics [7–17], quantum field theory, supersymmetric (SUSY) field theories [18], cavity optomechanics [19–26], quantum plasmonics [21, 27–29], light-induced superconductivity [30, 31], quantum thermodynamics [32], photochemistry (chemistry QED) [33–36], as well as metamaterial and material sciences. For a more detailed review, see Refs. [4, 5]. Ultrastrong coupling also has applications in quantum metrology and spectroscopy [37] and quantum information processing (QIP), including novel and efficient realizations of protected QIP [38], holonomic QIP [39], quantum gates [40, 41], quantum memories [42, 43], and quantum error correction codes [13].

The basic model for USC of a single two-level atom to a single-mode cavity is the quantum Rabi model [44, 45] (QRM). Its multi-atom or multi-mode generalizations include the Dicke [46] and Hopfield [47] models. When $\eta < 0.1$, these models for USC can be reduced to the simpler Jaynes-Cummings model [48] (JCM) and its multi-mode or multi-atom generalizations (e.g., the Tavis-Cummings model [49]). Since SC is easier to realize in experiment than USC, the question arises whether the predicted USC phenomena can

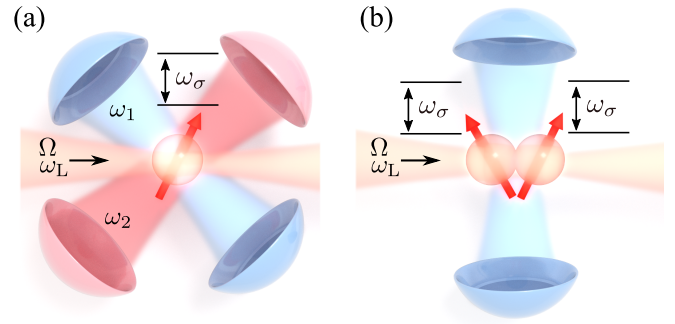


FIG. 1: Sketches of the two setups that we consider for observing ultrastrong-coupling phenomena. (a) A single two-level atom of frequency ω_σ coupled to two cavities of frequencies ω_1 and ω_2 . (b) Two two-level atoms of frequency ω_σ coupled to a cavity of frequency ω_a . In both setups, a single coherent drive of frequency ω_L and amplitude Ω is applied to each atom.

be observed or at least simulated also in the SC regime, e.g., by adding classical drives applied to atom(s) or cavity mode(s) in the SC models. We note that simulating the QRM could also enable simulating other closely related fundamental quantum models, which include the spin-boson [50, 51] and Kondo [50, 52, 53] renormalization-group models, the Rashba-Dresselhaus model [18], and a Jahn-Teller model [54–58]) among others. Even vacuum-induced symmetry breaking [59], which is analogous to the Higgs mechanism, has been predicted in the USC regime.

Quantum simulations are among the most important applications of quantum technologies [60, 61]. Quantum simulations of the atom-cavity dynamics in the USC and DSC regime in the Rabi and Dicke models have recently attracted much theoretical [62–74] and experimental [75–78] interest. The methods described in Refs. [63, 65] and implemented in circuit-QED [76] and trapped-ion experiments [78] simulate the QRM in the USC regime with a light-matter system described by the JCM in the SC regime. These quantum simula-

tions require *two* drives to be applied to a system with a *single* atom and a *single-mode* resonator.

In this Letter, we propose a method for quantum simulations of USC light-matter phenomena using only a *single* drive applied to a *multi-atom* or *multi-mode* system, as illustrated in Fig. 1. We show how this method can be used to simulate hallmark USC processes that do not conserve the number of excitations in the light-matter system [11]: a single two-level atom emitting two photons [8], frequency conversion of two photonic modes coupled to a two-level atom [12], and a single photon exciting two atoms [10]. We also give a protocol for an experimental implementation and show that several different well-developed experimental systems can be used for such an implementation. Given the breadth of USC research areas outlined above, we expect that this new simulation method will find many more applications.

Hamiltonians for light-matter coupling.—The QRM describes the interaction between a two-level atom (qubit) of frequency ω_a and a cavity mode of frequency ω_c by the Hamiltonian ($\hbar = 1$)

$$H_R = H_0 + \sigma_x X = H_0 + g(\sigma + \sigma^\dagger)(a + a^\dagger), \quad (1)$$

where $H_0 = (\omega_a/2)\sigma_z + \omega_c a^\dagger a$ is the free Hamiltonian, a (a^\dagger) is the annihilation (creation) operator of the cavity mode, $X = a + a^\dagger$ is the canonical position operator, $\sigma_x = \sigma + \sigma^\dagger$ and σ_z are Pauli operators, σ (σ^\dagger) is the atomic lowering (raising) operator, and g is the atom-field coupling constant. Under the rotating-wave approximation (RWA), which is valid if $\{\omega_c, \omega_a\} \gg \{g, |\omega_c - \omega_a|\}$, the counter-rotating terms, $\sigma^\dagger a^\dagger$ and σa , in Eq. (1) can be ignored. This leads to the standard JCM described by the Hamiltonian $H_{JC} = H_0 + g(\sigma a^\dagger + \sigma^\dagger a)$. The counter-rotating terms can be effectively restored in the JCM in various ways, e.g., using cavity-light squeezing [71, 72] to enhance the coupling strength g . A simpler method is to apply classical drives, as suggested in Ref. [63]. Indeed, by applying two time-dependent classical drives to the atom, $H_{\text{drv}} = \sum_{n=1,2} \Omega_n (\sigma e^{i\omega_n t} + \sigma^\dagger e^{-i\omega_n t})$, with driving strengths Ω_n and frequencies ω_n , in addition to H_{JC} , the effective interaction Hamiltonian H'_R can simulate the QRM [63]. Note that H'_R is given as an approximate interaction in a rotated frame (where the first drive is time independent and spins are in the basis rotated by the Hadamard gate), assuming that Ω_1 is relatively strong, and choosing the resonance condition for the second drive strength as $\Omega_2 = (\omega_1 - \omega_2)/2$. Under these assumptions and approximations, H'_R can be given by Eq. (1), but with a rescaled effective cavity frequency $\omega'_c = \omega_c - \omega_1$ and the effective coupling constant $g' = g/2$. Thus, the JCM with two classical drives can effectively simulate the QRM, where the ratio $\eta \equiv g/\omega_c$ can be effectively increased as $\eta' \equiv g'/\omega'_c = g/[2(\omega_c - \omega_1)]$ from the SC regime up to the USC regime, or even the DSC regime.

Here we show that, instead of simulating the QRM, we can enable particular nonlinear processes [8, 10–13] that have been reported in the USC, and that rely on the effect of counter-rotating terms, by using a simpler approach based on

a *single* driving field. Our approach is inspired by earlier work on creating multi-photon states in cavity QED [79–81].

USC effect I: Two photons excited by a single atom.—We first consider the setup in Fig. 1(a), i.e. two cavities coupled to a single qubit that is coherently driven by a classical field. In a frame rotating with the frequency ω_L of the driving field, the Hamiltonian is given by

$$H = \Delta_1 a_1^\dagger a_1 + \Delta_2 a_2^\dagger a_2 + \Delta_\sigma \sigma^\dagger \sigma + \Omega(\sigma + \sigma^\dagger) + g \left[\sigma (a_1^\dagger + a_2^\dagger) + \text{h.c.} \right], \quad (2)$$

with $a_{1,2}$ the bosonic annihilation operators of the cavity modes; Δ_1 , Δ_2 and Δ_σ are the frequency detunings between the cavities or qubit and the drive ($\Delta_x \equiv \omega_x - \omega_L$), Ω is the amplitude of the driving field, and g is the coupling rate between the cavities and the qubit (considered to be equal for simplicity).

The part of Eq. (2) that only depends on σ can be easily diagonalized. Denoting the ground and excited eigenstates of a non-driven qubit $|g\rangle$ and $|e\rangle$, respectively, the new eigenstates with the driving applied correspond to a rotated spin basis, i.e.

$$|+\rangle = \cos \theta |g\rangle + \sin \theta |e\rangle = e^{i\sigma_y 2\theta} |g\rangle, \quad (3)$$

$$|-\rangle = \sin \theta |g\rangle - \cos \theta |e\rangle = -e^{i\sigma_y (2\theta + \pi)} |g\rangle, \quad (4)$$

with $\cos \theta \equiv 1/\sqrt{1 + \xi^{-2}}$, $\sin \theta \equiv 1/\sqrt{1 + \xi^2}$, $\theta \in [0, \pi/2]$, and $\xi \equiv \Omega/(\Delta_\sigma/2 + R)$, where R is the Rabi frequency given by $R \equiv \sqrt{\Omega^2 + (\Delta_\sigma/2)^2}$.

Working in the eigenbasis $|\pm\rangle$, the original lowering operator σ can be written in terms of the new operators $\tilde{\sigma} \equiv |-\rangle\langle +|$ as $\sigma = s^2 \tilde{\sigma} - c^2 \tilde{\sigma}^\dagger + cs \tilde{\sigma}_z$, with $s = \sin \theta$, $c = \cos \theta$, $\tilde{\sigma}_z \equiv 2\tilde{\sigma}^\dagger \tilde{\sigma} - \mathbb{1}$. Therefore, the resulting Hamiltonian in the rotated spin basis reads

$$H = \Delta_1 a_1^\dagger a_1 + \Delta_2 a_2^\dagger a_2 + R \tilde{\sigma}_z + g \left[(s^2 \tilde{\sigma} - c^2 \tilde{\sigma}^\dagger + cs \tilde{\sigma}_z) (a_1^\dagger + a_2^\dagger) + \text{h.c.} \right]. \quad (5)$$

The transition energy of the effective qubit is now given by R , which can be made small enough that counter-rotating terms of the kind $\tilde{\sigma}^\dagger a_1^\dagger$ and $\tilde{\sigma}_z a_1^\dagger$ play a relevant role in the dynamics. The presence of the latter type of coupling terms, involving $\tilde{\sigma}_z$, makes H reminiscent of the generalized QRM, where a coupling term proportional to $\sigma_z(a + a^\dagger)$ is added to the QRM in Eq. (1) [7, 8, 10, 11, 82, 83]. The presence of the $\tilde{\sigma}_z$ coupling term breaks parity symmetry and enables processes that changes the number of excitations in the system by an odd number [4, 5, 11].

We will now see how, in the limit of $\alpha \equiv g/R \ll 1$, the counter-rotating terms in Eq. (5) lead to Rabi oscillations between pairs of eigenstates of the bare Hamiltonian that are *not* directly coupled by the interactions [11], with Rabi frequencies $\propto \alpha g$. In the effective USC regime when $\alpha \sim 0.1$, we find the optimal condition in which $g/R \ll 1$ remains valid, while the effective Rabi frequencies $\sim 0.1g$ can be significant compared to decoherence rates. The normal USC condition $\eta \gtrsim 0.1$ for observing these phenomena is thus lifted.

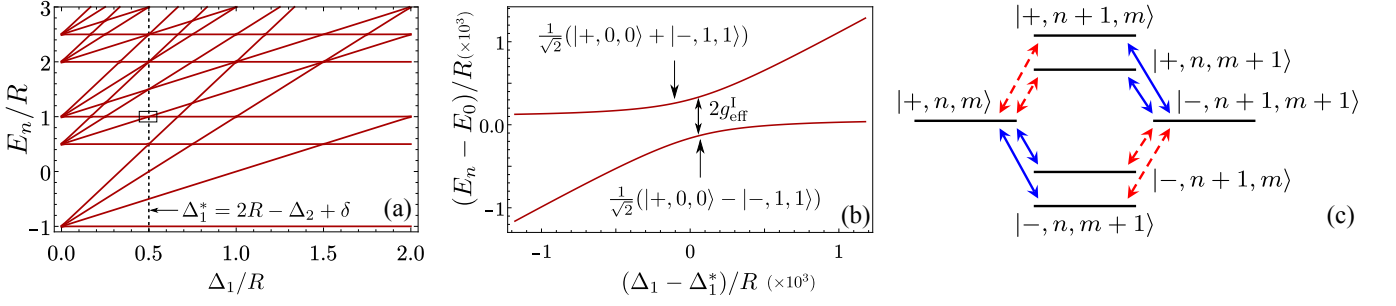


FIG. 2: USC effect I: Energy-level diagrams and transitions for the process where a single atom emits two photons. (a) Energy levels E_n for the Hamiltonian in Eq. (5) as a function of Δ_1 . Parameters: $\Omega = 80g$, $\Delta_\sigma = \Omega/\sqrt{2}$, $\Delta_2 = 3R/2$, with $R = \sqrt{\Omega^2 + \Delta_\sigma^2}/4$. The Hilbert space is truncated at three photons for simplicity. (b) Zoom-in on the anti-crossing between the energy levels corresponding to $|+, 0, 0\rangle$ and $|- , 1, 1\rangle$. The size of the level splitting at the resonance $\Delta_1 = \Delta_1^* \approx 2R - \Delta_2$ —where both states have the same energy in the absence of coupling $E_0 = \Delta_2 - R = R$ —indicates the strength g_{eff}^I of the effective interaction between these two states. (c) The transitions in the second-order process that creates the effective coupling between $|+, n, m\rangle$ and $|- , n + 1, m + 1\rangle$. Red dashed (blue solid) arrows indicate transitions that change the total number of excitations in the system by one (zero), i.e. transitions mediated by counter-rotating (non-rotating) terms. The transition cannot take place without involving counter-rotating terms.

One example of such a nonlinear process is the simultaneous excitation of one photon in each cavity by the single qubit. By plotting the energy levels of Eq. (5) [Fig. 2(a)], and zooming in around $\Delta_1 + \Delta_2 \approx 2R$, we find an avoided-level crossing [Fig. 2(b)]. The interaction around this point is described by the effective Hamiltonian [84]:

$$H_{\text{eff}}^I = \Delta_1 a_1^\dagger a_1 + \Delta_2 a_2^\dagger a_2 + (R + \lambda) \tilde{\sigma}_z + \left(\chi_1 a_1^\dagger a_1 + \chi_2 a_2^\dagger a_2 \right) \tilde{\sigma}_z + g_{\text{eff}}^I \left(a_1^\dagger a_2^\dagger \tilde{\sigma} + \text{h.c.} \right), \quad (6)$$

which couples the states $|+, n, m\rangle \leftrightarrow |- , n + 1, m + 1\rangle$, confining the dynamics inside that manifold. This effective interaction requires both states to be quasi-resonant, which implies, ignoring for now small dispersive energy shifts, the two conditions:

$$\Delta_1 + \Delta_2 \approx 2R, \quad (7a)$$

$$\Delta_1 \neq \Delta_2 \neq (\pm R, \pm 2R). \quad (7b)$$

The second condition is imposed in order to be detuned from first-order processes (e.g., $\tilde{\sigma} a_1^\dagger + \text{h.c.}$ if $\Delta_1 = 2R$) and competing second-order processes (e.g., $\tilde{\sigma} a_1^{\dagger 2} + \text{h.c.}$ for $\Delta_1 = R$) exciting degenerate photon pairs within a single cavity [79–81]. The effective two-photon coupling rate in Eq. (6) is given by

$$g_{\text{eff}}^I = \frac{g^2}{Rf(1-f)} cs^3, \quad (8)$$

where we defined $\Delta_1 = 2fR$ and $\Delta_2 = (1-f)2R$, $f \in (0, 1)$, so that Eq. (7a) is automatically fulfilled. This effective interaction is mediated by the second-order processes shown in Fig. 2(c). The Lamb shift of the qubit is

$$\lambda = g^2 \left[\frac{c^4}{2} \left(\frac{1}{\Delta_1^+} + \frac{1}{\Delta_2^+} \right) - \frac{s^4}{2} \left(\frac{1}{\Delta_1^-} + \frac{1}{\Delta_2^-} \right) \right], \quad (9)$$

and the dispersive coupling rates are

$$\chi_i = g^2 \left(\frac{c^4}{\Delta_i^+} - \frac{s^4}{\Delta_i^-} \right), \quad (10)$$

with $\Delta_i^\pm \equiv \Delta_i \pm 2R$.

Equation (8) shows that the resonant-driving condition $\Delta_\sigma = 0$ ($\theta = \pi/4$) does not provide the maximum possible two-photon coupling rate. In particular, for a fixed R , we see that the optimal angle θ maximizing g_{eff}^I is $\theta^* = \pi/3$. This angle yields the optimum value $g_{\text{eff}}^I(\theta^*) \approx 1.3g_{\text{eff}}^I(\theta = \pi/4)$. Alternatively, we can compute the optimal detuning Δ_σ for a fixed Ω , which is experimentally more meaningful since varying Δ_σ for a fixed Ω is more straightforward than varying θ for a fixed R . By writing Eq. (8) explicitly in terms of Δ_σ and Ω , we obtain the optimal detuning $\Delta_\sigma^* = \Omega/\sqrt{2}$. The corresponding value of g_{eff}^I is then given by $g_{\text{eff}}^I(\Delta_\sigma^*) \approx 1.18g_{\text{eff}}^I(\Delta_\sigma = 0)$.

In order to obtain full two-photon Rabi oscillations between the two states $|1\rangle = |+, n, m\rangle$, $|2\rangle = |- , n + 1, m + 1\rangle$, the quasi-resonance condition Eq. (7a) needs to be fine-tuned to account for the Lamb shift of the qubit and the dispersive qubit-cavity couplings in Eq. (6), given by λ and χ_1, χ_2 . In other words, Δ_1 and Δ_2 must be chosen such that $\langle 1|H_{\text{eff}}|1\rangle = \langle 2|H_{\text{eff}}|2\rangle$. Introducing a correction δ such that $\Delta_1 = 2Rf + \delta$, we solve this equation for the Hamiltonian in Eq. (6) and obtain

$$\delta = 2\lambda + \chi_1(2n + 1) + \chi_2(2m + 1). \quad (11)$$

Experimental protocol.—We now discuss an experimental protocol for implementing and measuring the non-linear process. This protocol is shown in Fig. 3. Starting with no photons in the cavities and the qubit in its ground state $|g\rangle$, the first step is to apply a rotation of 2θ around the y -axis to bring the qubit into the eigenstate $|+\rangle$. At this stage, the cavities and the qubit are detuned and no interaction takes place. Then, the

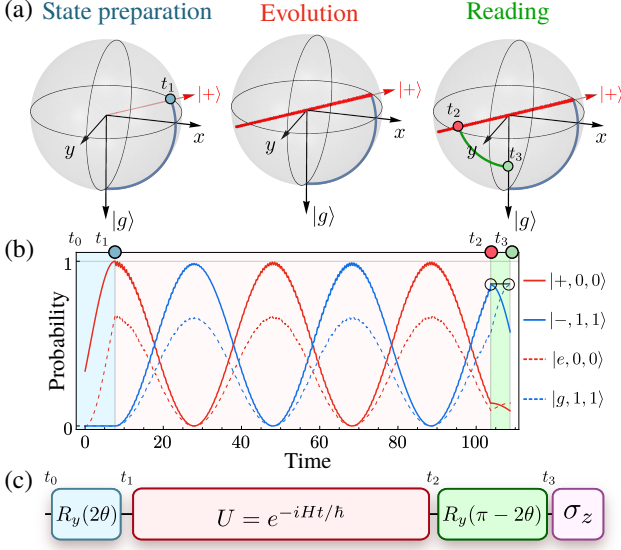


FIG. 3: USC effect I: Illustration of the experimental protocol, showing (a) the Bloch sphere picture of the qubit state, (b) the time evolution of the occupation probabilities for the most relevant states, and (c) a schematic diagram of the proposed pulse sequence. From time t_0 to t_1 , the qubit is rotated to the correct initial state in the rotated spin basis. From time t_1 to t_2 , the qubit is driven and the system evolves according to the Hamiltonian in Eq. (5), i.e., moving back and forth along the red trajectory depicted in the Bloch sphere. At time t_2 , the drive is turned off and the qubit is rotated back to the original basis, where it is then measured at time t_3 .

driving field is switched on and the nonlinear process becomes resonant. After the system has evolved for a time t , the drive is switched off (effectively decoupling the qubit and the cavity), and the state of the qubit in the $|\pm\rangle$ basis is transformed back into the $\{|g\rangle, |e\rangle\}$ basis (eigenstates of σ_z) by applying a rotation of $(\pi - 2\theta)$ around the y -axis. A measurement of the qubit population in the $\{|g\rangle, |e\rangle\}$ basis then reveals the qubit final state in the rotated basis.

USC effect II: Frequency conversion.—The setup in Fig. 1(a) can also be exploited to engineer other processes, e.g., frequency conversion. In that case, we want to couple the states $|n+1, m, -\rangle$ and $|n, m+1, +\rangle$. The resonance condition then becomes

$$\Delta_1 \approx 2R + \Delta_2, \quad (12a)$$

$$\Delta_1 \neq \Delta_2 \neq \pm R, \quad (12b)$$

where, again, the second condition guarantees that second-order processes introducing photon pairs into the cavities are off-resonance. Following the same procedure outlined in [84], we obtain the effective Hamiltonian

$$H_{\text{eff}}^{\text{II}} = \Delta_1 a_1^\dagger a_1 + \Delta_2 a_2^\dagger a_2 + (R + \lambda) \tilde{\sigma}_z + \left(\chi_1 a_1^\dagger a_1 + \chi_2 a_2^\dagger a_2 \right) \tilde{\sigma}_z + g_{\text{eff}}^{\text{II}} \left(a_1^\dagger a_2 \tilde{\sigma} + \text{h.c.} \right), \quad (13)$$

where the frequency-conversion rate is given by

$$g_{\text{eff}}^{\text{II}} = \frac{g^2 [(f-1)c^3 s + fcs^3]}{Rf(f-1)}, \quad (14)$$

having now defined $\Delta_1 = 2fR$ and $\Delta_2 = (f-1)2R$, $f \in (0, 1)$. Once again, driving the qubit on resonance does not maximize $g_{\text{eff}}^{\text{II}}$. Frequency-conversion-rate increases by 50-70% compared to resonant driving can be achieved by using the optimal angle θ^* or the optimal detuning Δ^* , whose analytical expressions can be found in the Supplemental Material [84].

USC effect III: Two atoms excited by a single photon.—The last process that we demonstrate is the excitation of two atoms by a single photon, i.e. the direct coupling between the states $|+, +, n\rangle$ and $|-, -, n+1\rangle$. We now consider the setup in Fig. 1(b), i.e. a cavity coupled to two coherently driven qubits, with lowering operators $\sigma_{1,2}$. For simplicity and without loss of generality, we consider both qubits to have the same transition frequencies. In the rotating frame of the driving, the Hamiltonian is

$$H = \Delta_a a^\dagger a + \Delta_\sigma (\sigma_1^\dagger \sigma_1 + \sigma_2^\dagger \sigma_2) + \Omega (\sigma_1 + \sigma_2 + \text{h.c.}) + g \left[a (\sigma_1^\dagger + \sigma_2^\dagger) + \text{h.c.} \right], \quad (15)$$

where a is the bosonic annihilation operator of the cavity, and $\Delta_a = \omega_a - \omega_L$ ($\Delta_\sigma = \omega_\sigma - \omega_L$) is the cavity (qubit) detuning from the drive frequency. In the dressed-qubits basis, the resonance condition enabling the desired non-linear process simply reads $\Delta_a \approx 4R$. We then obtain [84] the effective Hamiltonian

$$H_{\text{eff}}^{\text{III}} = \Delta_a a^\dagger a + \sum_i (R + \lambda) \tilde{\sigma}_{z,i} + \chi a^\dagger a \tilde{\sigma}_{z,i} + g_{\text{eff}}^{\text{III}} \left(a^\dagger \sigma_1 \sigma_2 + a \sigma_1^\dagger \sigma_2^\dagger \right), \quad (16)$$

with an effective coupling rate that emerges from third-order processes,

$$g_{\text{eff}}^{\text{III}} = \frac{g^3}{3R^2} (c^3 s^3 + 3cs^5). \quad (17)$$

As in the previous cases, the effective coupling can be maximized by driving the qubit slightly off resonance, using either the optimal angle θ^* or the optimal detuning Δ^* , whose expressions we provide in [84].

Experimental implementations.—The results presented here are based on very fundamental models that describe the exchange of single excitations between a qubit and a harmonic oscillator, and can therefore be applied in many different systems. In Table I, we compare, under experimentally feasible assumptions, the effective coupling strengths g_{eff} and decoherence rates γ that can be obtained in five experimental platforms. An experimental implementation is feasible when $g_{\text{eff}}/\gamma > 1$, i.e. when the effective coupling is strong. Table I shows that the second-order processes we have proposed

System	$g/(2\pi)$	$\gamma/(2\pi)$	$(g_{\text{eff}}^{\text{I}}, g_{\text{eff}}^{\text{II}}, g_{\text{eff}}^{\text{III}})/\gamma$
Natural atoms [85]	34 MHz	4.1 MHz	(0.6, 0.4, 0.004)
Trapped ions [86]	10 kHz	100 Hz	(7.9, 5.1, 0.05)
Quantum acoustics [87]	16 MHz	0.6 MHz	(2.1, 1.3, 0.01)
Circuit QED [88]	335 MHz	0.5 MHz	(52.9, 33.8, 0.36)
Quantum dots [89]	19.3 GHz	6.0 GHz	(0.3, 0.2, 0.002)

TABLE I: Experimentally feasible effective rates for the three processes discussed in the text: (I) a single photon exciting two atoms, (II) frequency conversion, and (III) a single atom exciting two photons. We set $\Omega/g = 20$; γ refers to the largest decoherence rate in the system.

here should be ready for implementation in several systems, and the third-order process may be within reach for circuit-QED setups. However, we note that the nonlinear processes may also be exploited even in the dissipative regime where $g_{\text{eff}} < \gamma$, e.g. yielding multi-photon emission with non-classical properties [79–81, 90].

Conclusions.—We have presented a experimentally simple method for quantum simulations of phenomena in the USC regime, requiring only a single qubit drive to be applied on a system in the SC regime. Our method is ready for its implementation on several existing experimental platforms and opens up new possibilities for exploring USC physics.

Acknowledgements. C.S.M. is funded by the Marie Skłodowska-Curie Fellowship QUSON (Project No. 752180). F.N. acknowledges partial support from the MURI Center for Dynamic Magneto-Optics via the Air Force Office of Scientific Research (AFOSR) award No. FA9550-14-1-0040, the Army Research Office (ARO) under grant No. W911NF-18-1-0358, the Asian Office of Aerospace Research and Development (AOARD) grant No. FA2386-18-1-4045, the Japan Science and Technology Agency (JST) [through the Q-LEAP program, the IMPACT program, and CREST Grant No. JP-MJCR1676, the Japan Society for the Promotion of Science (JSPS) through the JSPS-RFBR grant No. 17-52-50023 and the JSPS-FWO grant No. VS.059.18N], the RIKEN-AIST Challenge Research Fund, the FQXi and the NTT PHI Labs.

[1] S. Haroche, *Nobel Lecture: Controlling photons in a box and exploring the quantum to classical boundary*, *Rev. Mod. Phys.* **85**, 1083 (2013).
[2] X. Gu, A. F. Kockum, A. Miranowicz, Y.-X. Liu, and F. Nori, *Microwave photonics with superconducting quantum circuits*, *Phys. Rep.* **718-719**, 1 (2017), arXiv:1707.02046.
[3] A. F. Kockum and F. Nori, *Quantum Bits with Josephson Junctions*, in *Fundamentals and Frontiers of the Josephson Effect*, edited by F. Tafuri (Springer, 2019) pp. 703–741, arXiv:1908.09558.
[4] A. F. Kockum, A. Miranowicz, S. De Liberato, S. Savasta, and F. Nori, *Ultrastrong coupling between light and matter*, *Nat. Rev. Phys.* **1**, 19 (2019), arXiv:1807.11636.
[5] P. Forn-Díaz, L. Lamata, E. Rico, J. Kono, and E. Solano, *Ultrastrong coupling regimes of light-matter interaction*, *Rev.*

Mod. Phys. **91**, 025005 (2019), arXiv:1804.09275.
[6] J. Casanova, G. Romero, I. Lizuain, J. J. García-Ripoll, and E. Solano, *Deep Strong Coupling Regime of the Jaynes-Cummings Model*, *Phys. Rev. Lett.* **105**, 263603 (2010), arXiv:1008.1240.
[7] T. Niemczyk, F. Deppe, H. Huebl, E. P. Menzel, F. Hocke, M. J. Schwarz, J. J. Garcia-Ripoll, D. Zueco, T. Hümmer, E. Solano, A. Marx, and R. Gross, *Circuit quantum electrodynamics in the ultrastrong-coupling regime*, *Nat. Phys.* **6**, 772 (2010), arXiv:1003.2376.
[8] L. Garziano, R. Stassi, V. Macrì, A. F. Kockum, S. Savasta, and F. Nori, *Multiphoton quantum Rabi oscillations in ultrastrong cavity QED*, *Phys. Rev. A* **92**, 063830 (2015), arXiv:1509.06102.
[9] K. K. W. Ma and C. K. Law, *Three-photon resonance and adiabatic passage in the large-detuning Rabi model*, *Phys. Rev. A* **92**, 023842 (2015).
[10] L. Garziano, V. Macrì, R. Stassi, O. Di Stefano, F. Nori, and S. Savasta, *One Photon Can Simultaneously Excite Two or More Atoms*, *Phys. Rev. Lett.* **117**, 043601 (2016), arXiv:1601.00886.
[11] A. F. Kockum, V. Macrì, L. Garziano, S. Savasta, and F. Nori, *Frequency conversion in ultrastrong cavity QED*, *Sci. Rep.* **7**, 5313 (2017), arXiv:1701.07973.
[12] A. F. Kockum, A. Miranowicz, V. Macrì, S. Savasta, and F. Nori, *Deterministic quantum nonlinear optics with single atoms and virtual photons*, *Phys. Rev. A* **95**, 063849 (2017), arXiv:1701.05038.
[13] R. Stassi, V. Macrì, A. F. Kockum, O. Di Stefano, A. Miranowicz, S. Savasta, and F. Nori, *Quantum nonlinear optics without photons*, *Phys. Rev. A* **96**, 023818 (2017), arXiv:1702.00660.
[14] O. Di Stefano, R. Stassi, L. Garziano, A. F. Kockum, S. Savasta, and F. Nori, *Feynman-diagrams approach to the quantum Rabi model for ultrastrong cavity QED: stimulated emission and re-absorption of virtual particles dressing a physical excitation*, *New J. Phys.* **19**, 053010 (2017), arXiv:1603.04984.
[15] O. Di Stefano, A. F. Kockum, A. Ridolfo, S. Savasta, and F. Nori, *Photodetection probability in quantum systems with arbitrarily strong light-matter interaction*, *Sci. Rep.* **8**, 17825 (2018), arXiv:1711.10698.
[16] V. Macrì, F. Nori, and A. F. Kockum, *Simple preparation of Bell and Greenberger-Horne-Zeilinger states using ultrastrong-coupling circuit QED*, *Phys. Rev. A* **98**, 062327 (2018), arXiv:1810.09808.
[17] L. Cong, S. Felicetti, J. Casanova, L. Lamata, E. Solano, and I. Arrazola, *Selective Interactions in the Quantum Rabi Model*, (2019), arXiv:1908.07358.
[18] M. Tomka, M. Pletyukhov, and V. Gritsev, *Supersymmetry in quantum optics and in spin-orbit coupled systems*, *Sci. Rep.* **5**, 13097 (2015), arXiv:1407.5213.
[19] L. Garziano, R. Stassi, V. Macrì, S. Savasta, and O. Di Stefano, *Single-step arbitrary control of mechanical quantum states in ultrastrong optomechanics*, *Phys. Rev. A* **91**, 023809 (2015).
[20] J.-M. Pirkkalainen, S. Cho, F. Massel, J. Tuorila, T. Heikkilä, P. Hakonen, and M. Sillanpää, *Cavity optomechanics mediated by a quantum two-level system*, *Nat. Commun.* **6**, 6981 (2015), arXiv:1412.5518.
[21] F. Benz, M. K. Schmidt, A. Dreismann, R. Chikkaraddy, Y. Zhang, A. Demetriadou, C. Carnegie, H. Ohadi, B. de Nijs, R. Esteban, J. Aizpurua, and J. J. Baumberg, *Single-molecule optomechanics in “picocavities”*, *Science* **354**, 726 (2016).
[22] V. Macrì, L. Garziano, A. Ridolfo, O. Di Stefano, and S. Savasta, *Deterministic synthesis of mechanical NOON states in ultrastrong optomechanics*, *Phys. Rev. A* **94**, 013817 (2016).

- [23] M. Cirio, K. Debnath, N. Lambert, and F. Nori, *Amplified Optomechanical Transduction of Virtual Radiation Pressure*, *Phys. Rev. Lett.* **119**, 053601 (2017), arXiv:1612.02953 .
- [24] V. Macrì, A. Ridolfo, O. Di Stefano, A. F. Kockum, F. Nori, and S. Savasta, *Nonperturbative Dynamical Casimir Effect in Optomechanical Systems: Vacuum Casimir-Rabi Splittings*, *Phys. Rev. X* **8**, 011031 (2018), arXiv:1706.04134 .
- [25] O. Di Stefano, A. Settinieri, V. Macrì, A. Ridolfo, R. Stassi, A. F. Kockum, S. Savasta, and F. Nori, *Interaction of Mechanical Oscillators Mediated by the Exchange of Virtual Photon Pairs*, *Phys. Rev. Lett.* **122**, 030402 (2019), arXiv:1712.00121 .
- [26] A. Settinieri, V. Macrì, L. Garziano, O. Di Stefano, F. Nori, and S. Savasta, *Conversion of mechanical noise into correlated photon pairs: Dynamical Casimir effect from an incoherent mechanical drive*, *Phys. Rev. A* **100**, 022501 (2019), arXiv:1903.00878 .
- [27] M. S. Tame, K. R. McEnery, S. K. Özdemir, J. Lee, S. A. Maier, and M. S. Kim, *Quantum plasmonics*, *Nat. Phys.* **9**, 329 (2013), arXiv:1312.6806 .
- [28] F. Todisco, M. De Giorgi, M. Esposito, L. De Marco, A. Zizzari, M. Bianco, L. Dominici, D. Ballarini, V. Arima, G. Gigli, and D. Sanvitto, *Ultrastrong Plasmon-Exciton Coupling by Dynamic Molecular Aggregation*, *ACS Photonics* **5**, 143 (2018).
- [29] B. Munkhbat, M. Wersäll, D. G. Baranov, T. J. Antosiewicz, and T. Shegai, *Suppression of photo-oxidation of organic chromophores by strong coupling to plasmonic nanoantennas*, *Sci. Adv.* **4**, eaas9552 (2018).
- [30] M. A. Sentef, M. Ruggenthaler, and A. Rubio, *Cavity quantum-electrodynamical polaritonically enhanced electron-phonon coupling and its influence on superconductivity*, *Sci. Adv.* **4**, eaau6969 (2018), arXiv:1802.09437 .
- [31] F. Schlawin, A. Cavalleri, and D. Jaksch, *Cavity-Mediated Electron-Photon Superconductivity*, *Phys. Rev. Lett.* **122**, 133602 (2019), arXiv:1804.07142 .
- [32] S. Seah, S. Nimmrichter, and V. Scarani, *Refrigeration beyond weak internal coupling*, *Phys. Rev. E* **98**, 012131 (2018), arXiv:1803.02002 .
- [33] J. Galego, F. J. Garcia-Vidal, and J. Feist, *Cavity-Induced Modifications of Molecular Structure in the Strong-Coupling Regime*, *Phys. Rev. X* **5**, 041022 (2015), arXiv:1506.03331 .
- [34] F. Herrera and F. C. Spano, *Cavity-Controlled Chemistry in Molecular Ensembles*, *Phys. Rev. Lett.* **116**, 238301 (2016), arXiv:1512.05017 .
- [35] T. W. Ebbesen, *Hybrid Light-Matter States in a Molecular and Material Science Perspective*, *Acc. Chem. Res.* **49**, 2403 (2016).
- [36] L. A. Martínez-Martínez, R. F. Ribeiro, J. Campos-González-Angulo, and J. Yuen-Zhou, *Can Ultrastrong Coupling Change Ground-State Chemical Reactions?* *ACS Photonics* **5**, 167 (2018), arXiv:1705.10655 .
- [37] M. Ruggenthaler, N. Tancogne-Dejean, J. Flick, H. Appel, and A. Rubio, *From a quantum-electrodynamical light-matter description to novel spectroscopies*, *Nat. Rev. Chem.* **2**, 0118 (2018).
- [38] P. Nataf and C. Ciuti, *Protected Quantum Computation with Multiple Resonators in Ultrastrong Coupling Circuit QED*, *Phys. Rev. Lett.* **107**, 190402 (2011), arXiv:1106.1159 .
- [39] Y. Wang, J. Zhang, C. Wu, J. Q. You, and G. Romero, *Holonomic quantum computation in the ultrastrong-coupling regime of circuit QED*, *Phys. Rev. A* **94**, 012328 (2016), arXiv:1605.05449 .
- [40] G. Romero, D. Ballester, Y. M. Wang, V. Scarani, and E. Solano, *Ultrafast Quantum Gates in Circuit QED*, *Phys. Rev. Lett.* **108**, 120501 (2012), arXiv:1110.0223 .
- [41] Y. Wang, C. Guo, G.-Q. Zhang, G. Wang, and C. Wu, *Ultrafast quantum computation in ultrastrongly coupled circuit QED systems*, *Sci. Rep.* **7**, 44251 (2017).
- [42] T. H. Kyaw, S. Felicetti, G. Romero, E. Solano, and L.-C. Kwek, *Scalable quantum memory in the ultrastrong coupling regime*, *Sci. Rep.* **5**, 8621 (2015), arXiv:1404.5778 .
- [43] R. Stassi and F. Nori, *Long-lasting quantum memories: Extending the coherence time of superconducting artificial atoms in the ultrastrong-coupling regime*, *Phys. Rev. A* **97**, 033823 (2018), arXiv:1703.08951 .
- [44] I. I. Rabi, *On the Process of Space Quantization*, *Phys. Rev.* **49**, 324 (1936).
- [45] I. I. Rabi, *Space Quantization in a Gyration Magnetic Field*, *Phys. Rev.* **51**, 652 (1937).
- [46] R. H. Dicke, *Coherence in Spontaneous Radiation Processes*, *Phys. Rev.* **93**, 99 (1954).
- [47] J. J. Hopfield, *Theory of the Contribution of Excitons to the Complex Dielectric Constant of Crystals*, *Phys. Rev.* **112**, 1555 (1958).
- [48] E. T. Jaynes and F. W. Cummings, *Comparison of quantum and semiclassical radiation theories with application to the beam maser*, *Proc. IEEE* **51**, 89 (1963).
- [49] M. Tavis and F. W. Cummings, *Exact Solution for an N-Molecule-Radiation-Field Hamiltonian*, *Phys. Rev.* **170**, 379 (1968).
- [50] K. Le Hur, *Kondo resonance of a microwave photon*, *Phys. Rev. B* **85**, 140506 (2012), arXiv:1104.0708 .
- [51] J. Leppäkangas, J. Braumüller, A. V. Ustinov, M. Weides, and M. Marthaler, *Quantum simulation of the spin-boson model in a microwave circuit*, *Phys. Rev. A* (2018), arXiv:1711.07463 .
- [52] M. Goldstein, M. H. Devoret, M. Houzet, and L. I. Glazman, *Inelastic Microwave Photon Scattering off a Quantum Impurity in a Josephson-Junction Array*, *Phys. Rev. Lett.* **110**, 017002 (2013), arXiv:1208.0319 .
- [53] I. Snyman and S. Florens, *Robust Josephson-Kondo screening cloud in circuit quantum electrodynamics*, *Phys. Rev. B* **92**, 085131 (2015), arXiv:1503.05708 .
- [54] A. P. Hines, C. M. Dawson, R. H. McKenzie, and G. J. Milburn, *Entanglement and bifurcations in Jahn-Teller models*, *Phys. Rev. A* **70**, 022303 (2004), arXiv:0402016 [quant-ph] .
- [55] C. P. Meaney, T. Duty, R. H. McKenzie, and G. J. Milburn, *Jahn-Teller instability in dissipative quantum systems*, *Phys. Rev. A* **81**, 043805 (2010).
- [56] J. Larson, *Jahn-Teller systems from a cavity QED perspective*, *Phys. Rev. A* **78**, 033833 (2008), arXiv:0804.4416 .
- [57] J. Bourassa, J. M. Gambetta, A. A. Abdumalikov, O. Astafiev, Y. Nakamura, and A. Blais, *Ultrastrong coupling regime of cavity QED with phase-biased flux qubits*, *Phys. Rev. A* **80**, 032109 (2009), arXiv:0906.1383 .
- [58] T. Dereli, Y. Gül, P. Forn-Díaz, and Ö. E. Müstecaplıoğlu, *Two-frequency Jahn-Teller systems in circuit QED*, *Phys. Rev. A* **85**, 053841 (2012), arXiv:1109.1199 .
- [59] L. Garziano, R. Stassi, A. Ridolfo, O. Di Stefano, and S. Savasta, *Vacuum-induced symmetry breaking in a superconducting quantum circuit*, *Phys. Rev. A* **90**, 043817 (2014), arXiv:1406.5119 .
- [60] I. Buluta and F. Nori, *Quantum Simulators*, *Science* **326**, 108 (2009).
- [61] I. M. Georgescu, S. Ashhab, and F. Nori, *Quantum simulation*, *Rev. Mod. Phys.* **86**, 153 (2014), arXiv:1308.6253 .
- [62] F. Dimer, B. Estienne, A. S. Parkins, and H. J. Carmichael, *Proposed realization of the Dicke-model quantum phase transition in an optical cavity QED system*, *Phys. Rev. A* **75**, 013804 (2007), arXiv:0607115 [quant-ph] .

- [63] D. Ballester, G. Romero, J. J. García-Ripoll, F. Deppe, and E. Solano, *Quantum Simulation of the Ultrastrong-Coupling Dynamics in Circuit Quantum Electrodynamics*, *Phys. Rev. X* **2**, 021007 (2012), [arXiv:1107.5748](#).
- [64] A. L. Grimsmo and S. Parkins, *Cavity-QED simulation of qubit-oscillator dynamics in the ultrastrong-coupling regime*, *Phys. Rev. A* **87**, 033814 (2013), [arXiv:1212.6063](#).
- [65] J. S. Pedernales, I. Lizuain, S. Felicetti, G. Romero, L. Lamata, and E. Solano, *Quantum Rabi Model with Trapped Ions*, *Sci. Rep.* **5**, 15472 (2015), [arXiv:1505.00698](#).
- [66] S. Felicetti, J. S. Pedernales, I. L. Egusquiza, G. Romero, L. Lamata, D. Braak, and E. Solano, *Spectral collapse via two-phonon interactions in trapped ions*, *Phys. Rev. A* **92**, 033817 (2015), [arXiv:1506.00493](#).
- [67] R. Puebla, M.-J. Hwang, J. Casanova, and M. B. Plenio, *Probing the Dynamics of a Superradiant Quantum Phase Transition with a Single Trapped Ion*, *Phys. Rev. Lett.* **118**, 073001 (2017), [arXiv:1607.03781](#).
- [68] S. Fedortchenko, S. Felicetti, D. Marković, S. Jezouin, A. Keller, T. Coudreau, B. Huard, and P. Milman, *Quantum simulation of ultrastrongly coupled bosonic modes using superconducting circuits*, *Phys. Rev. A* **95**, 042313 (2017), [arXiv:1612.05542](#).
- [69] X. Wang, A. Miranowicz, H.-R. Li, and F. Nori, *Observing pure effects of counter-rotating terms without ultrastrong coupling: A single photon can simultaneously excite two qubits*, *Phys. Rev. A* **96**, 063820 (2017), [arXiv:1709.05199](#).
- [70] I. Aedo and L. Lamata, *Analog quantum simulation of generalized Dicke models in trapped ions*, *Phys. Rev. A* **97**, 042317 (2018), [arXiv:1802.01853](#).
- [71] W. Qin, A. Miranowicz, P.-B. Li, X.-Y. Lü, J.-Q. You, and F. Nori, *Exponentially Enhanced Light-Matter Interaction, Cooperativities, and Steady-State Entanglement Using Parametric Amplification*, *Phys. Rev. Lett.* **120**, 093601 (2018), [arXiv:1709.09555](#).
- [72] C. Leroux, L. C. G. Govia, and A. A. Clerk, *Enhancing Cavity Quantum Electrodynamics via Antisqueezing: Synthetic Ultrastrong Coupling*, *Phys. Rev. Lett.* **120**, 093602 (2018), [arXiv:1709.09091](#).
- [73] N. Lambert, M. Cirio, M. Delbecq, G. Allison, M. Marx, S. Tarucha, and F. Nori, *Amplified and tunable transverse and longitudinal spin-photon coupling in hybrid circuit-QED*, *Phys. Rev. B* **97**, 125429 (2018), [arXiv:1712.02077](#).
- [74] A. Di Paolo, P. K. Barkoutsos, I. Tavernelli, and A. Blais, *Variational Quantum Simulation of Ultrastrong Light-Matter Coupling*, (2019), [arXiv:1909.08640](#).
- [75] A. Crespi, S. Longhi, and R. Osellame, *Photonic Realization of the Quantum Rabi Model*, *Phys. Rev. Lett.* **108**, 163601 (2012), [arXiv:1111.6424](#).
- [76] J. Braumüller, M. Marthaler, A. Schneider, A. Stehli, H. Rotzinger, M. Weides, and A. V. Ustinov, *Analog quantum simulation of the Rabi model in the ultra-strong coupling regime*, *Nat. Commun.* **8**, 779 (2017), [arXiv:1611.08404](#).
- [77] N. K. Langford, R. Sagastizabal, M. Kounalakis, C. Dickel, A. Bruno, F. Luthi, D. J. Thoen, A. Endo, and L. DiCarlo, *Experimentally simulating the dynamics of quantum light and matter at deep-strong coupling*, *Nat. Commun.* **8**, 1715 (2017), [arXiv:1610.10065](#).
- [78] D. Lv, S. An, Z. Liu, J.-N. Zhang, J. S. Pedernales, L. Lamata, E. Solano, and K. Kim, *Quantum Simulation of the Quantum Rabi Model in a Trapped Ion*, *Phys. Rev. X* **8**, 021027 (2018), [arXiv:1711.00582](#).
- [79] C. Sánchez Muñoz, E. del Valle, A. González Tudela, K. Müller, S. Lichtmannecker, M. Kaniber, C. Tejedor, J. J. Finley, and F. P. Laussy, *Emitters of N-photon bundles*, *Nat. Photonics* **8**, 550 (2014), [arXiv:1306.1578](#).
- [80] C. Sánchez Muñoz, F. P. Laussy, C. Tejedor, and E. del Valle, *Enhanced two-photon emission from a dressed biexciton*, *New J. Phys.* **17**, 123021 (2015), [arXiv:1506.05050](#).
- [81] C. Sánchez Muñoz, F. P. Laussy, E. del Valle, C. Tejedor, and A. González-Tudela, *Filtering multiphoton emission from state-of-the-art cavity quantum electrodynamics*, *Optica* **5**, 14 (2018), [arXiv:1707.03690](#).
- [82] F. Deppe, M. Mariantoni, E. P. Menzel, A. Marx, S. Saito, K. Kakuyanagi, H. Tanaka, T. Meno, K. Semba, H. Takayanagi, E. Solano, and R. Gross, *Two-photon probe of the Jaynes-Cummings model and controlled symmetry breaking in circuit QED*, *Nat. Phys.* **4**, 686 (2008), [arXiv:0805.3294](#).
- [83] F. Yoshihara, T. Fuse, S. Ashhab, K. Kakuyanagi, S. Saito, and K. Semba, *Superconducting qubit-oscillator circuit beyond the ultrastrong-coupling regime*, *Nat. Phys.* **13**, 44 (2017), [arXiv:1602.00415](#).
- [84] Supplementary Material.
- [85] K. M. Birnbaum, A. Boca, R. Miller, A. D. Boozer, T. E. Northup, and H. J. Kimble, *Photon blockade in an optical cavity with one trapped atom*, *Nature* **436**, 87 (2005).
- [86] H. Häffner, C. F. Roos, and R. Blatt, *Quantum computing with trapped ions*, *Phys. Rep.* **469**, 155 (2008), [arXiv:0809.4368](#).
- [87] P. Arrangoiz-Arriola, E. A. Wollack, Z. Wang, M. Pechal, W. Jiang, T. P. McKenna, J. D. Witmer, R. Van Laer, and A. H. Safavi-Naeini, *Resolving the energy levels of a nanomechanical oscillator*, *Nature* **571**, 537 (2019), [arXiv:1902.04681](#).
- [88] P. Magnard, P. Kurpiers, B. Royer, T. Walter, J.-C. Besse, S. Gasparinetti, M. Pechal, J. Heinsoo, S. Storz, A. Blais, and A. Wallraff, *Fast and Unconditional All-Microwave Reset of a Superconducting Qubit*, *Phys. Rev. Lett.* **121**, 060502 (2018), [arXiv:1801.07689](#).
- [89] Y. Arakawa, S. Iwamoto, M. Nomura, A. Tandraechanurat, and Y. Ota, *Cavity Quantum Electrodynamics and Lasing Oscillation in Single Quantum Dot-Photonic Crystal Nanocavity Coupled Systems*, *IEEE J. Sel. Top. Quantum Electron.* **18**, 1818 (2012).
- [90] Y. Chang, A. González-Tudela, C. Sánchez Muñoz, C. Navarrete-Benlloch, and T. Shi, *Deterministic Down-Converter and Continuous Photon-Pair Source within the Bad-Cavity Limit*, *Phys. Rev. Lett.* **117**, 203602 (2016).

Supplementary Material

Contents

Effective Hamiltonians	8
USC effect I: Details for two photons excited by a single atom	9
USC effect II: Details for frequency conversion	9
USC effect III: Details for two atoms excited by a single photon	10
Validity of the perturbation theory	11
Effect of decoherence	12

Effective Hamiltonians

In this work, we use a matrix form of perturbation theory that allows one to obtain energy corrections to arbitrary orders with a single matrix inversion. Let us consider a Hilbert subspace \mathcal{A} consisting of \mathcal{N}_A states $\{|a_1\rangle, |a_2\rangle, \dots\}$ whose effective dynamics we wish to describe. This subspace is coupled to another subspace \mathcal{B} consisting of \mathcal{N}_B states $\{|b_1\rangle, |b_2\rangle, \dots\}$ that we want to adiabatically eliminate. We define the projectors onto the respective subspaces as P_A and P_B . The total Hamiltonian of the combined system is given by

$$H = \begin{pmatrix} h & V \\ V^\dagger & \tilde{H} \end{pmatrix}, \quad (\text{S1})$$

where $h \equiv P_A H P_A$ is an $(N_A \times N_A)$ matrix acting only on \mathcal{A} , $\tilde{H} \equiv P_B H P_B$ is an $(N_B \times N_B)$ matrix acting only on \mathcal{B} , and $V \equiv P_B H P_A$ is an $(N_A \times N_B)$ matrix coupling both subspaces. Our objective is to obtain an effective Hamiltonian h^{eff} describing the dynamics within \mathcal{A} . The underlying assumption is that the eigenvalues of h are close to the energy E , while the eigenvalues of \tilde{H} are detuned from E by values much larger than the elements of V , and therefore can be adiabatically eliminated. This is done by writing the eigenvalue problem:

$$\begin{pmatrix} h & V \\ V^\dagger & \tilde{H} \end{pmatrix} \begin{pmatrix} \phi \\ \chi \end{pmatrix} = E \begin{pmatrix} \phi \\ \chi \end{pmatrix}, \quad (\text{S2})$$

where ϕ and χ are column vectors of length N_A and N_B , respectively. After matrix multiplication, we obtain the following system of two equations for ϕ and χ :

$$(E - h)\phi = V\chi, \quad (\text{S3a})$$

$$(E - \tilde{H})\chi = V^\dagger\phi. \quad (\text{S3b})$$

By solving Eq. (S3b) and substituting into Eq. (S3a), we obtain:

$$(E - H_{\text{eff}})\phi = 0, \quad (\text{S4})$$

where $H_{\text{eff}}(E) = h + \delta h$, and

$$\delta h = V \frac{1}{E - \tilde{H}} V^\dagger. \quad (\text{S5})$$

H_{eff} corresponds to effective Hamiltonians that we have presented in the main text. Notably, this simple expression includes contributions from processes beyond second-order perturbation theory; the order of such processes is encoded in the *size* of the matrix. In the following sections we provide further details on how the effective Hamiltonian was obtained in the three cases studied in the main text.

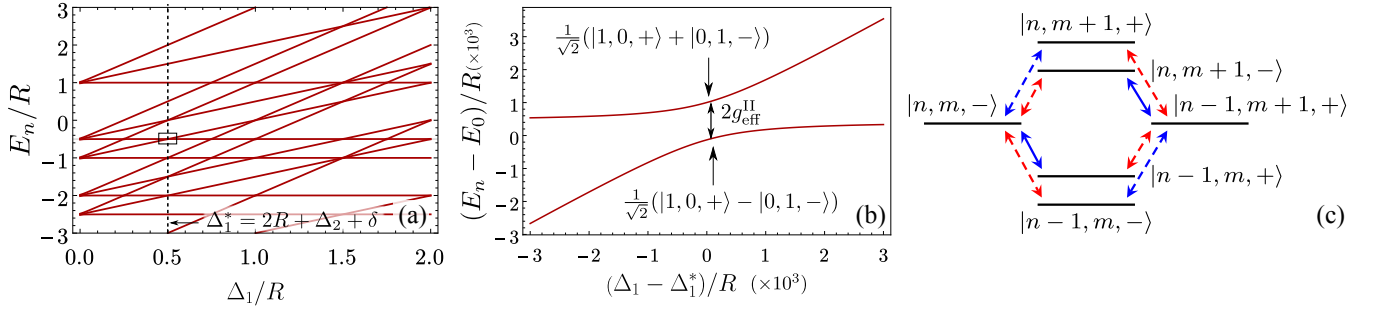


FIG. S1: USC effect II: Energy-level diagrams and transitions for the process of frequency conversion. (a) Energy levels E_n for the Hamiltonian in Eq. (5) as a function of Δ_1 . Parameters: $\Omega = 40g$, $\Delta_\sigma = \Delta_\sigma^*$ [see Eq. (S14)], $\Delta_2 = 2R(f-1)$, with $f = 1/4$ and $R = \sqrt{\Omega^2 + \Delta_\sigma^2}/4$. The Hilbert space is truncated at 1 photon for simplicity. (b) Zoom-in on the anti-crossing between the energy levels corresponding to $|1, 0, +\rangle$ and $|0, 1, -\rangle$. The size of the level splitting at the resonance $\Delta_1 = \Delta_1^* = 2R + \Delta_2 + \delta = 2Rf + \delta$ —where both states have the same energy in the absence of coupling $E_0 = \Delta_2 + R = R(2f - 1)$ —indicates the strength $g_{\text{eff}}^{\text{II}}$ of the effective interaction between these two states. (c) The transitions in the second-order process that creates the effective coupling between $|n, m, -\rangle$ and $|n-1, m+1, +\rangle$. Blue solid arrows: transitions that conserve the number of excitations. Red dashed arrows: transitions that change the number of excitations by one. Blue dashed arrows: transitions that change the number of excitations by two.

USC effect I: Details for two photons excited by a single atom

We consider the following two subspaces, with $N_A = 2$ and $N_B = 12$:

- $\mathcal{A} = \{|n, m, +\rangle, |n+1, m+1, -\rangle\}$,
- $\mathcal{B} = \{|n+1, m, \pm\rangle, |n, m+1, \pm\rangle, |n+2, m+1, \pm\rangle, |n+1, m+2, \pm\rangle, |n, m-1, \pm\rangle, |n-1, m, \pm\rangle\}$.

Note that states such as $|n+2, m+1, \pm\rangle$ do not contribute to the effective coupling between the two states in \mathcal{A} , but to the Lamb shifts and dispersive cavity-qubit couplings, through processes such as $|n+1, m+1, -\rangle \rightarrow |n+2, m+1, \pm\rangle \rightarrow |n+1, m+1, -\rangle$. For simplicity, those processes are neither depicted in Fig. 2 of the main text nor in Fig. S1 and S2. Using $E = \Delta_1 n + \Delta_2 m + R$, the correction to the effective Hamiltonian in the subspace \mathcal{A} , given by Eq. (S5), has the form:

$$\delta h^{\text{I}} = \begin{pmatrix} \chi_1 n + \chi_2 m + \lambda + C & g_{\text{eff}}^{\text{I}} \sqrt{(n+1)(m+1)} \\ g_{\text{eff}}^{\text{I}} \sqrt{(n+1)(m+1)} & -\chi_1(n+1) - \chi_2(m+1) - \lambda + C \end{pmatrix}, \quad (\text{S6})$$

which allows us to extract χ_1 , χ_2 , λ and $g_{\text{eff}}^{\text{I}}$, and, omitting any overall shift C , to write the effective Hamiltonian $H_{\text{eff}}^{\text{I}}$ in the general form

$$H_{\text{eff}}^{\text{I}} = \Delta_1 a_1^\dagger a_1 + \Delta_2 a_2^\dagger a_2 + (R + \lambda) \tilde{\sigma}_z + \left(\chi_1 a_1^\dagger a_1 + \chi_2 a_2^\dagger a_2 \right) \tilde{\sigma}_z + g_{\text{eff}}^{\text{I}} \left(a_1^\dagger a_2^\dagger \tilde{\sigma} + \text{h.c.} \right).$$

The expressions for $g_{\text{eff}}^{\text{I}}$, χ_1 , χ_2 and λ are provided in the main text.

USC effect II: Details for frequency conversion

We consider the following two subspaces, with $N_A = 2$ and $N_B = 12$:

- $\mathcal{A} = \{|n+1, m, -\rangle, |n, m+1, +\rangle\}$,
- $\mathcal{B} = \{|n+1, m+1, \pm\rangle, |n, m, \pm\rangle, |n+2, m, \pm\rangle, |n+1, m-1, \pm\rangle, |n, m+2, \pm\rangle, |\pm, n-1, m\rangle\}$

Here, the correction that we obtain is

$$\delta h^{\text{II}} = \begin{pmatrix} -(n+1)\chi_1 - m\chi_2 - \lambda + C & g_{\text{eff}}^{\text{II}} \sqrt{(n+1)(m+1)} \\ g_{\text{eff}}^{\text{II}} \sqrt{(n+1)(m+1)} & n\chi_1 + (m+1)\chi_2 + \lambda + C \end{pmatrix}, \quad (\text{S7})$$

which allows us to write the general form of the effective Hamiltonian,

$$H_{\text{eff}}^{\text{II}} = \Delta_1 a_1^\dagger a_1 + \Delta_2 a_2^\dagger a_2 + (R + \lambda) \tilde{\sigma}_z + \left(\chi_1 a_1^\dagger a_1 + \chi_2 a_2^\dagger a_2 \right) \tilde{\sigma}_z + g_{\text{eff}}^{\text{II}} \left(a_1^\dagger a_2 \tilde{\sigma} + \text{h.c.} \right).$$

The expression for $g_{\text{eff}}^{\text{II}}$ is given in the main text. The dispersive coupling rates are in this case given by

$$\chi_i = g^2 \left(\frac{c^4}{2R + \Delta_i} + \frac{s^4}{2R - \Delta_i} \right), \quad (\text{S8})$$

and the Lamb shift is

$$\lambda = \frac{g^2}{2} \left[\frac{c^4(4R + \Delta_1 + \Delta_2)}{(2R + \Delta_1)(2R + \Delta_2)} + \frac{s^4(4R - \Delta_1 - \Delta_2)}{(2R - \Delta_1)(2R - \Delta_2)} \right]. \quad (\text{S9})$$

The dispersive couplings and the Lamb shift make the diagonal elements of δh^{II} unequal. Since both elements need to be equal in order to achieve complete Rabi oscillations, one needs to introduce a small correction the resonance condition $\Delta_1 + \Delta_2 = 2R$. Introducing the correction δ such that $\Delta_1 = 2Rf + \delta$ into the final expression of H_{eff} (which implies the approximation of ignoring δ during the derivation of H_{eff}), and imposing that the diagonal elements are equal, we are left with the expression for the correction to the general resonance condition:

$$\delta = (2n + 1)\chi_1 + (2m + 1)\chi_2 + 2\lambda. \quad (\text{S10})$$

This expression in terms of χ_i and λ coincides with the one obtained for the case of two photons excited by a single atom. Similarly, driving the qubit on resonance does not maximize $g_{\text{eff}}^{\text{II}}$ either. Optimizing the angle gives

$$\theta^*(f \lesssim \frac{1}{2}) = \arccos \left[\frac{\sqrt{3 + 2f \pm \sqrt{9 - 4f + 4f^2}}}{2\sqrt{2}} \right]. \quad (\text{S11})$$

The factor gained with respect to $\theta = \pi/4$ is also f -dependent and has the following expression:

$$\frac{g_{\text{eff}}^{\text{II}}(\theta^*)}{g_{\text{eff}}^{\text{II}}(\theta = \pi/4)} = -\frac{(-6f + f' + 3) \sqrt{-2f(2f + f' - 2) + f' + 3}}{8\sqrt{2}(2f - 1)} \quad (\text{S12})$$

where $f' = \sqrt{4(f - 1)f + 9}$. For the particular case $f = 1/4$, we find

$$g_{\text{eff}}^{\text{II}}(\theta^*) \approx 1.76 g_{\text{eff}}^{\text{II}}(\theta = \pi/4). \quad (\text{S13})$$

Alternatively, we can compute the optimal detuning Δ_σ for a fixed Ω (instead of fixed R), which is experimentally more meaningful given that varying Δ_σ for a fixed Ω is more straightforward than varying θ for a fixed R :

$$\Delta_\sigma^* = -\Omega \frac{(1 - 2f)}{|1 - 2f|} \sqrt{-2 + \frac{1 - \sqrt{1 - f(1 - f)}|1 - 2f|}{f(1 - f)}}. \quad (\text{S14})$$

For the particular case $f = 1/4$, $\Delta_\sigma^* \approx -0.96 \Omega$, which leads to

$$g_{\text{eff}}^{\text{II}}(\Delta_\sigma^*) \approx 1.52 g_{\text{eff}}^{\text{II}}(\Delta_\sigma = 0). \quad (\text{S15})$$

USC effect III: Details for two atoms excited by a single photon

We consider the following two subspaces, with $N_{\mathcal{A}} = 2$ and $N_{\mathcal{B}} = 12$:

- $\mathcal{A} = \{|+, +, n\rangle, |-, -, n + 1\rangle\}$,
- $\mathcal{B} = \{|+, -, n + 1\rangle, |-, +, n + 1\rangle, |+, +, n + 1\rangle, |+, -, n\rangle, |-, +, n\rangle, |-, -, n\rangle, |+, -, n + 2\rangle, |-, +, n + 2\rangle, |-, -, n + 2\rangle, |-, +, n - 1\rangle, |+, -, n - 1\rangle, |+, +, n - 1\rangle\}$.

Here, the correction that we obtain is

$$\delta h^{\text{III}} = \begin{pmatrix} 2n\chi + 2\lambda + C & g_{\text{eff}}^{\text{III}}\sqrt{n+1} \\ g_{\text{eff}}^{\text{III}}\sqrt{n+1} & -2(n+1)\chi - 2\lambda + C \end{pmatrix}. \quad (\text{S16})$$

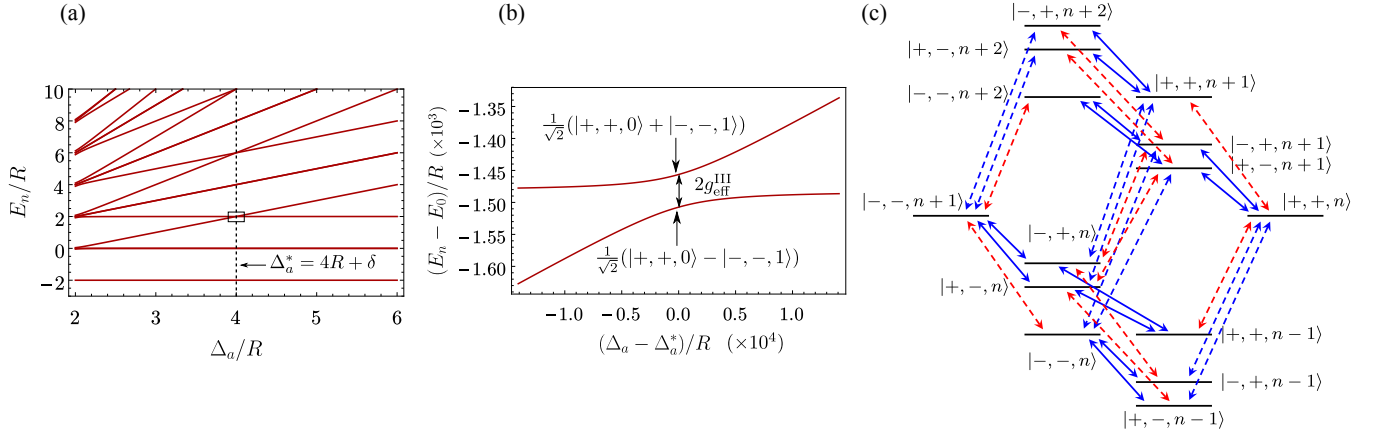


FIG. S2: USC effect III: Energy-level diagrams and transitions for the process of exciting two atoms with a single photon. (a) Energy levels E_n for the Hamiltonian in Eq. (15) as a function of Δ_a . Parameters: $\Omega = 20g$, $\Delta_\sigma = \Delta_\sigma^*$ [see Eq. (S21)], with $R = \sqrt{\Omega^2 + \Delta_\sigma^2}/4$. The Hilbert space is truncated at 4 photons for simplicity. (b) Zoom-in on the anti-crossing between the energy levels corresponding to $|+, +, 0\rangle$ and $|-, -, 1\rangle$. The size of the level splitting at the resonance $\Delta_a = \Delta_a^* = 4R + \delta$ —where both states have the same energy in the absence of coupling $E_0 = 2R$ —indicates the strength $g_{\text{eff}}^{\text{III}}$ of the effective interaction between these two states. (c) The transitions in the third-order process that creates the effective coupling between $|-, -, n+1\rangle$ and $|+, +, n-1\rangle$. Blue solid arrows: transitions that conserve the number of excitations. Red dashed arrows: transitions that change the number of excitations by one. Blue dashed arrows: transitions that change the number of excitations by two.

The dispersive coupling and the Lamb shift are given by second-order processes:

$$\chi = g^2 \frac{(2R - \Delta_a)c^4 + (2R + \Delta_a)s^4}{4R^2 - \Delta_a^2}, \quad (\text{S17})$$

$$\lambda = \chi/2. \quad (\text{S18})$$

Setting $\Delta_a = 4R + \delta$, the optimum resonance condition is given by

$$\delta = (4n + 2)\chi + 4\lambda = 4(n + 1)\chi. \quad (\text{S19})$$

For a fixed R , we can see that the optimal angle θ maximizing g_{eff} is $\theta^* = \arctan\left(\sqrt{\frac{1+\sqrt{5}}{3-\sqrt{5}}}\right) \approx 0.356\pi$, giving the following maximum value of $g_{\text{eff}}^{\text{III}}$:

$$g_{\text{eff}}^{\text{III}}(\theta^*) = \sqrt{\frac{11 + 5\sqrt{5}}{8}} \frac{g^3}{6R^2} \approx 1.67g_{\text{eff}}^{\text{III}}(\theta = \pi/4). \quad (\text{S20})$$

That is, when choosing the optimal angle θ^* we obtain $1.67\times$ enhancement with respect to the resonant case $\Delta_\sigma = 0$, which corresponds to $\theta = \pi/4$. In a similar way, we can express this in terms of the optimal detuning:

$$\Delta_\sigma^* = \Omega \sqrt{\frac{14\sqrt{109} - 122}{45}} \approx 0.73\Omega. \quad (\text{S21})$$

The corresponding value of g_{eff} is then given by

$$g_{\text{eff}}^{\text{III}}(\Delta_\sigma^*) \approx -1.3 \frac{g^3}{6\Omega^2} = 1.3g_{\text{eff}}^{\text{III}}(\Delta_\sigma = 0) \quad (\text{S22})$$

giving $1.3\times$ enhancement with respect to the resonant case, for the same driving amplitude Ω .

Validity of the perturbation theory

In this section, we address the question of the validity of the perturbation theory for the three studied USC effects for large values of the perturbation parameter g/Ω . To do so, we study the energy-level splitting ΔE_k between the two eigenstates $|\varphi_k\rangle$

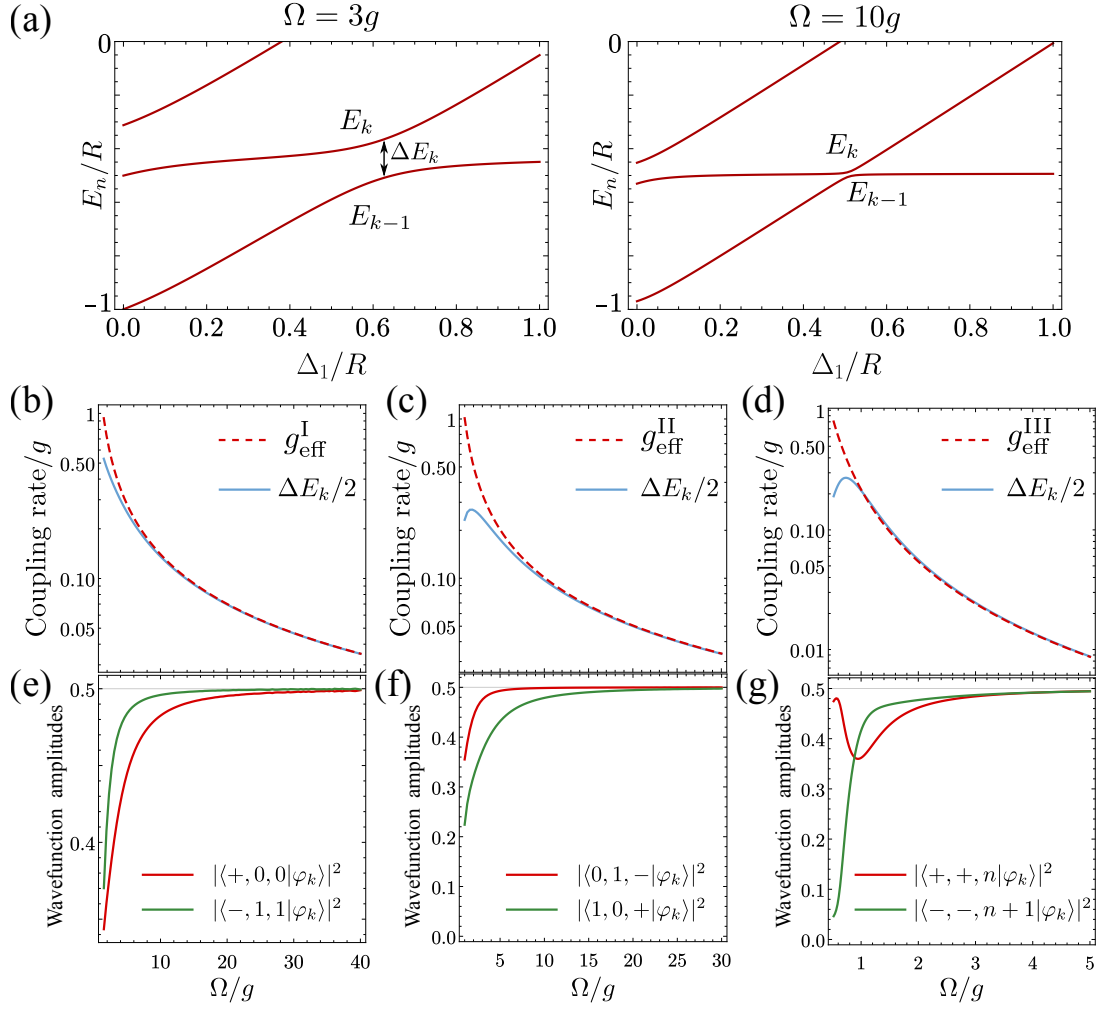


FIG. S3: Validity of the applied perturbation theory for the three examples. (a) Examples of the avoided crossings at two different values of the perturbation parameter g/Ω . Smaller values of Ω imply larger splitting. (b-c) Splitting at the avoided crossing (solid) versus Ω/g , compared to the effective rates computed from perturbation theory (dashed). The perturbation theory works when the two curves overlap. (e-f) The overlap between the two eigenstates at the avoided crossing and the two states involved in the nonlinear process; when the perturbation theory starts failing, the overlap is reduced, meaning that eigenstates contain contributions from other states.

and $|\varphi_{k-1}\rangle$ at the avoided-level crossing that we associate to each nonlinear process, see Fig. S3 (a). The resulting splitting is compared to the effective coupling rates $g_{\text{eff}}^{\text{I}}$, $g_{\text{eff}}^{\text{II}}$ and $g_{\text{eff}}^{\text{III}}$ that we have computed from perturbation theory, as we show in Fig. S3 (b-c). In addition, we compute the overlap between the two eigenstates $|\varphi_{k/k-1}\rangle$ and the two states between which we expect the Rabi oscillations to occur in each of the three cases considered in the text, see Fig. S3 (e-g). As Ω/g is reduced, the effective coupling rates increase. The perturbation theory starts failing at $\Omega/g \lesssim 10$ for cases I and II, and $\Omega/g \lesssim 2$ for case III (which is a third-order process). Below these values of Ω/g , $|\varphi_{k,k-1}\rangle$ stop being composed exclusively of the two isolated states that constitute the desired nonlinear process, and the effective coupling rate predicted from perturbation theory departs from the real half-splittings between these eigenstates.

Effect of decoherence

Here we provide further study of the effect of decoherence (beyond Table I in the main text) computing the dynamics of the nonlinear processes in the presence of cavity losses. This is done by using the standard Lindblad master equation for the

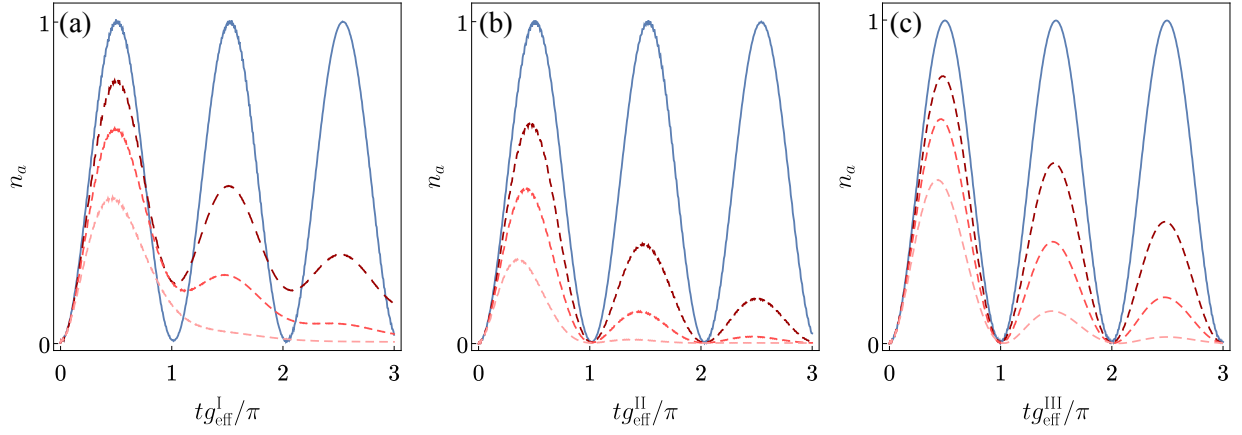


FIG. S4: Effect of decoherence induced by radiative decay in the cavity modes for the three nonlinear processes considered in this work. In each case, we monitor the population $n_a = \langle a^\dagger a \rangle$ of a cavity undergoing Rabi oscillations under the nonlinear processes with and without decay. Lossless dynamics are represented by straight, blue curves. Dissipative dynamics are shown in dashed curves, with lighter color representing higher decay rates. Decay rates used are $g_{\text{eff}} \times (0.25, 0.5, 1)$. $\Omega/g = 20$ (a), 20 (b) and 10 (c).

dynamics of the density matrix:

$$\dot{\rho} = -i[H, \rho] + \frac{\gamma_a}{2} \sum_{i=1}^{N_{\text{cav}}} \left(2a_i \rho a_i - a_i^\dagger a_i \rho - \rho a_i^\dagger a_i \right). \quad (\text{S23})$$

where γ_a is a cavity decay rate, and the sum runs over the total number of cavities (two in cases I and II, one in case III). In Fig. S4 we show that the effect of decoherence is the expected damping of the Rabi oscillations. The apparent higher robustness to losses of case III (two atoms excited by a single photon) can be explained by the fact that there is only one cavity, which is the only lossy subsystem, as compared to two cavities in cases I and II. We have assumed the cavity decay to be the main decoherence mechanism, therefore ignoring the decay or dephasing of the atoms to simplify the discussion.